Dyadic Green's Functions for an Anisotropic, Non-Local Model of Biased Graphene

George W. Hanson, *Senior Member, IEEE*

***Abstract*—Dyadic Green's functions are presented for an anisotropic surface conductivity model of biased graphene. The graphene surface can be biased using either a perpendicular static electric field, or by a static magnetic field via the Hall effect. The graphene is represented by an infinitesimally-thin, two-sided, non-local anisotropic conductivity surface, and the field is obtained in terms of Sommerfeld integrals. The role of spatial dispersion is accessed, and the effect of various static bias fields on electromagnetic field behavior is examined. It is shown that by varying the bias one can exert significant control over graphene's electromagnetic propagation characteristics, including guided surface wave phenomena, which may be useful for future electronic and photonic device applications.**

***Index Terms*—Dyadic Green's functions, electromagnetic theory, nanotechnology.**

I. Introduction

GRAPHENE, which is a planar atomic layer of carbon atoms bonded in a hexagonal structure, is a very promising material in emerging nanoelectronic applications [1]. Graphene is the two-dimensional version of graphite, and is related to carbon nanotubes in that a single-wall carbon nanotube can be thought of as a graphene sheet rolled into a cylinder [2].

Graphene's band structure, together with it's extreme thinness, leads to pronounced electric field and Hall effects [3]–[7], and to the possibility of various electronic devices [8], [9]. Intrinsic graphene is a zero bandgap semiconductor, and its conductivity can be tuned by either electrostatic or magnetostatic gating. Since this is the governing principle behind traditional semiconductor devices, this effect in graphene is particularly promising for the development of ultrathin carbon nanoelectronic devices. Although both the electric field effect and Hall effect can occur in atomically thin metal films, these tend to be thermodynamically unstable, and don't form continuous layers with good transport properties. In contrast, graphene is stable, and, like its cylindrical carbon nanotube versions, can exhibit ballistic transport over at least submicron distances [3].

Only recently has it become possible to fabricate actual graphene [3]–[7], although it has long been theoretically studied as a way to explain properties of graphite [10], and later, carbon nanotubes [2]. In graphene, the energy-momentum relationship for electrons is linear over a wide range of energies, rather then quadratic as in most materials, so that electrons in graphene behave as massless relativistic particles (Dirac fermions) with an energy-independent velocity. The linear energy bands lead to interesting quantum properties, and to a minimum conductivity even when charge carrier concentrations vanish [4].

In this work, the interaction of an electromagnetic current source and electrically or magnetically biased graphene at the interface between two materials is examined. Several situations are discussed: I) the role of spatial dispersion (non-locality), which leads to a tensor conductivity; II) effects due to electrostatic bias fields, which result in a scalar conductivity; and III) effects due to magnetostatic bias fields, which lead to a tensor conductivity. Some simple expressions are obtained for surface wave dispersion of graphene in a homogeneous medium.

The paper is organized as follows. In the body of the paper, dyadic Green's functions for the structure are presented, along with associated results. Appendix I provides the formulas for graphene's conductivity. In Appendix II, the intraband, spatially-dispersive conductivity is derived, and Appendix III briefly presents an alternative dyadic Green's function formulation that was found to be useful. This work follows that in [11], where an isotropic model of graphene was considered. All units are in the SI system, and the time variation (suppressed) is $e^{j\omega t}$, where j is the imaginary unit.

II. Formulation of the Model

A. Electronic Model of Graphene

Fig. 1 depicts laterally-infinite graphene lying in the $x-z$ plane at the interface between two different mediums characterized by μ_1, ε_1 for $z \geq 0$ and μ_2, ε_2 for $z < 0$, where all material parameters may be complex-valued.

The graphene sheet is modeled as an infinitesimally-thin, non-local two-sided surface characterized by a surface conductivity tensor obtained from microscopic, semi-classical and quantum mechanical considerations. This model of graphene follows from the two-sided conductivity surface approach developed in [12] for carbon nanotubes, and was applied to local isotropic graphene in [11]. Here the model is extended to the non-local anisotropic case

$$\underline{\boldsymbol{\sigma}}\,(\omega, \mu_c(\mathbf{E}_0), \Gamma, T, \mathbf{B}_0) = \hat{\mathbf{x}}\hat{\mathbf{x}}\sigma_{xx} + \hat{\mathbf{x}}\hat{\mathbf{y}}\sigma_{xy} + \hat{\mathbf{y}}\hat{\mathbf{x}}\sigma_{yx} + \hat{\mathbf{y}}\hat{\mathbf{y}}\sigma_{yy} \tag{1}$$

where ω is radian frequency, μ_c is the chemical potential [which can be controlled by an applied electrostatic bias field $\mathbf{E}_0 = \hat{\mathbf{z}}E_0$, or by doping; see the discussion of (51)], Γ is a phenomenological electron scattering rate that is assumed to be independent of energy, T is temperature, and $\mathbf{B_0} = \hat{\mathbf{z}}B_0$ is an applied magnetostatic bias field. In the following, the dependence

Manuscript received July 23, 2007; revised October 7, 2007.

The author is with the Department of Electrical Engineering, University of Wisconsin-Milwaukee, Milwaukee, WI 53211 USA (e-mail: george@uwm.edu).

Color versions of one or more of the figures in this paper are available online at http://ieeexplore.ieee.org.

Digital Object Identifier 10.1109/TAP.2008.917005

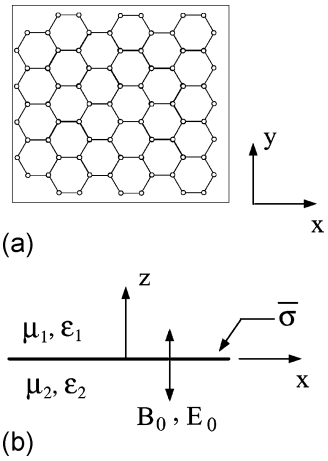

Fig. 1. (a) Depiction of graphene (top view), where the small circles denote carbon atoms, and (b) an anisotropic graphene sheet characterized by tensor conductance $\overline{\boldsymbol{\sigma}}$ at the interface between two dielectrics (side view). $\mathbf{B}_0$ and $\mathbf{E}_0$ denote possible dc bias fields.

on ω, Γ, and T will be suppressed. Three special cases of (1) will be considered.

I) Spatial dispersion, but neither electrostatic nor magnetostatic bias ($E_0 = B_0 = 0$). In this case the conductivity components become operators

$$\begin{aligned}\sigma_{xx} &= \sigma + \alpha\frac{d^2}{dx^2} + \beta\frac{d^2}{dy^2}\\ \sigma_{yy} &= \sigma + \beta\frac{d^2}{dx^2} + \alpha\frac{d^2}{dy^2}\\ \sigma_{xy} &= \sigma_{yx} = 2\beta\frac{d^2}{dxdy}\end{aligned} \tag{2}$$

where σ, α, and β are derived from the semi-classical Boltzmann's equation in Appendix II (see (96)–(101) for the final expressions).

II) Electrostatic bias, although no magnetostatic bias nor spatial dispersion ($E_0 \neq 0$, $B_0 = 0$). In this case the conductivity is a scalar

$$\begin{aligned}\sigma_{xx} &= \sigma_{yy} = \sigma_d\left(\mu_c(E_0)\right)\\ \sigma_{xy} &= \sigma_{yx} = 0\end{aligned} \tag{3}$$

where σ_d is given by (57) in Appendix I (equivalently, by (54), although this form converges very slowly as $B_0 \to 0$).

III) Magnetostatic bias, and possibly electrostatic bias, but no spatial dispersion ($B_0 \neq 0$, and possibly $E_0 \neq 0$). We refer to this as the local Hall effect regime, and in this case the conductivity tensor can be written as

$$\begin{aligned}\sigma_{xx} &= \sigma_{yy} = \sigma_d\left(\mu_c(E_0), B_0\right)\\ \sigma_{xy} &= -\sigma_{yx} = \sigma_o\left(\mu_c(E_0), B_0\right)\end{aligned} \tag{4}$$

where the conductivities σ_d and σ_o are given by (54) and (55) in Appendix I.

B. Dyadic Green's Function for a Surface Model of Graphene

In this section, a method for obtaining dyadic Green's functions for a general two-dimensional anisotropic surface will be presented, although due to space limitations explicit results will only be provided for the local Hall effect regime. The method of obtaining the Green's dyadics follows [13], adapted to the surface impedance case, and the resulting Green's functions are believed to be new.

For any planarly layered, piecewise-constant medium, the electric and magnetic fields in region n due to an electric current can be obtained as [14], [15]

$$\mathbf{E}^{(n)}(\mathbf{r}) = \left(k_n^2 + \boldsymbol{\nabla}\boldsymbol{\nabla}\cdot\right)\boldsymbol{\pi}^{(n)}(\mathbf{r}) \tag{5}$$

$$\mathbf{H}^{(n)}(\mathbf{r}) = j\omega\varepsilon_n\boldsymbol{\nabla}\times\boldsymbol{\pi}^{(n)}(\mathbf{r}) \tag{6}$$

where $k_n = \omega\sqrt{\mu_n\varepsilon_n}$ and $\boldsymbol{\pi}^{(n)}(\mathbf{r})$ are the wavenumber and electric Hertzian potential in region n, respectively. Assuming that the current source is in region 1, then

$$\boldsymbol{\pi}^{(1)}(\mathbf{r}) = \boldsymbol{\pi}_1^p(\mathbf{r}) + \boldsymbol{\pi}_1^s(\mathbf{r}) \tag{7}$$

$$= \int_\Omega \left\{\underline{\mathbf{g}}^p(\mathbf{r},\mathrm{r}') + \underline{\mathbf{g}}^r(\mathbf{r},\mathrm{r}')\right\}\cdot\frac{\mathbf{J}^{(1)}(\mathbf{r}')}{j\omega\varepsilon_1}d\Omega' \tag{8}$$

$$\boldsymbol{\pi}^{(2)}(\mathbf{r}) = \boldsymbol{\pi}_2^s(\mathbf{r}) = \int_\Omega \underline{\mathbf{g}}^t(\mathbf{r},\mathbf{r}')\cdot\frac{\mathbf{J}^{(1)}(\mathbf{r}')}{j\omega\varepsilon_1}d\Omega' \tag{9}$$

where the underscore indicates a dyadic quantity, and where Ω is the support of the current. With z parallel to the interface normal, the principle Greens dyadic can be written as [14]

$$\underline{\mathbf{g}}^p(\mathbf{r},\mathbf{r}') = \underline{\mathbf{I}}\frac{e^{-jk_1R}}{4\pi R} \tag{10}$$

$$= \underline{\mathbf{I}}\frac{1}{(2\pi)^2}\int_{-\infty}^{\infty}\int_{-\infty}^{\infty}\frac{e^{-p_1|z-z'|}}{2p_1}e^{-j\mathbf{q}\cdot(\mathbf{r}-\mathbf{r}')}dq_xdq_y \tag{11}$$

where

$$\mathbf{q} = \hat{\mathbf{x}}q_x + \hat{\mathbf{y}}q_y, \quad q_\rho = |\mathbf{q}| = \sqrt{q_x^2+q_y^2} \tag{12}$$

$$p_n^2 = q_\rho^2 - k_n^2, \quad \rho = \sqrt{(x-x')^2+(y-y')^2}$$

$$R = |\mathbf{r}-\mathbf{r}'| = \sqrt{\rho^2+(z-z')^2} \tag{13}$$

and where $\underline{\mathbf{I}}$ is the unit dyadic.

The scattered Green's dyadics can be obtained by enforcing the boundary conditions

$$\begin{aligned}\hat{\mathbf{z}}\times(\mathbf{H}_1-\mathbf{H}_2) &= \mathbf{J}_e^s\\ \hat{\mathbf{z}}\times(\mathbf{E}_1-\mathbf{E}_2) &= -\mathbf{J}_m^s\end{aligned} \tag{14}$$

where $\mathbf{J}_e^s$ (A/m) and $\mathbf{J}_m^s$ (V/m) are electric and magnetic surface currents on the boundary. In our case, $\mathbf{J}_m^s = \mathbf{0}$, and $\mathbf{J}_e^s = \underline{\boldsymbol{\sigma}}\cdot\mathbf{E}$. Introducing the two-dimensional Fourier transform

$$\mathbf{a}(\mathbf{q},z) = \int_{-\infty}^{\infty}\int_{-\infty}^{\infty}\mathbf{a}(\mathbf{r})e^{jq\cdot\mathbf{r}}dxdy \tag{15}$$

$$\mathbf{a}(\mathbf{r}) = \frac{1}{(2\pi)^2}\int_{-\infty}^{\infty}\int_{-\infty}^{\infty}\mathbf{a}(\mathbf{q},z)e^{-jq\cdot\mathbf{r}}dq_x dq_y \tag{16}$$

(14) becomes

$$\begin{aligned}
&k_1^2\pi_{1x} - jq_x\nabla\cdot\pi_1 \\
&\quad = k_2^2\pi_{2x} - jq_x\nabla\cdot\pi_2 &(17)\\
&k_1^2\pi_{1y} - jq_y\nabla\cdot\pi_1 \\
&\quad = k_2^2\pi_{2y} - jq_y\nabla\cdot\pi_2 &(18)\\
&j\omega\varepsilon_2\left(\frac{\partial\pi_{2x}}{\partial z} + jq_x\pi_{2z}\right) - j\omega\varepsilon_1\left(\frac{\partial\pi_{1x}}{\partial z} + jq_x\pi_{1z}\right) \\
&\quad = \sigma_{xx}\left(k_1^2\pi_{1x} - jq_x\nabla\cdot\pi_1\right) \\
&\qquad + \sigma_{xy}\left(k_1^2\pi_{1y} - jq_y\nabla\cdot\pi_1\right), &(19)\\
&j\omega\varepsilon_2\left(jq_y\pi_{2z} + \frac{\partial\pi_{2y}}{\partial z}\right) - j\omega\varepsilon_1\left(jq_y\pi_{1z} + \frac{\partial\pi_{1y}}{\partial z}\right) \\
&\quad = \sigma_{yx}\left(k_1^2\pi_{1x} - jq_x\nabla\cdot\pi_1\right) \\
&\qquad + \sigma_{yy}\left(k_1^2\pi_{1y} - jq_y\nabla\cdot\pi_1\right) &(20)
\end{aligned}$$

where

$$\nabla\cdot\pi = -jq_x\pi_x - jq_y\pi_y + \frac{\partial}{\partial z}\pi_z. \tag{21}$$

In the case of an isotropic surface, a vertical current maintains only a vertical potential, and a horizontal current induces both a horizontal and vertical potential [11], which is also the case for an isotropic layered medium in the absence of surface conductivity [13]. However, in the case of an anisotropic surface, a vertical current induces both a vertical and horizontal potential. That is, π_z alone cannot satisfy the boundary conditions, and, therefore, the pair (π_x, π_z) is relevant for both vertical currents and x-directed horizontal currents, and the pair (π_y, π_z) is relevant for vertical currents and y-directed horizontal currents. In each case the boundary conditions can be satisfied. The pair (π_x, π_z) reduce (17)–(20) to

$$\begin{aligned}
\pi_{1x} &= M^2N^2\pi_{2x} &(22)\\
\frac{\partial\pi_{1z}}{\partial z} - \frac{\partial\pi_{2z}}{\partial z} &= -jq_x(1-M^2N^2)\pi_{2x} &(23)\\
\omega q_x(\varepsilon_2\pi_{2z} - \varepsilon_1\pi_{1z}) &= -\left(\sigma_{xx}\left(k_1^2 - q_x^2\right) - \sigma_{xy}q_xq_y\right)\pi_{1x} \\
&\quad + (\sigma_{xx}jq_x + \sigma_{xy}jq_y)\frac{\partial\pi_{1z}}{\partial z} \\
&\quad - j\omega\left(\varepsilon_1\frac{\partial\pi_{1x}}{\partial z} - \varepsilon_2\frac{\partial\pi_{2x}}{\partial z}\right) &(24)\\
\omega q_y(\varepsilon_2\pi_{2z} - \varepsilon_1\pi_{1z}) &= -\left(\sigma_{yx}\left(k_1^2 - q_x^2\right) - \sigma_{yy}q_xq_y\right)\pi_{1x} \\
&\quad + (\sigma_{yx}jq_x + \sigma_{yy}jq_y)\frac{\partial\pi_{1z}}{\partial z} &(25)
\end{aligned}$$

with a similar reduction for the pair (π_y, π_z), where $N^2 = \varepsilon_2/\varepsilon_1$ and $M^2 = \mu_2/\mu_1$.

Enforcing the boundary conditions and following the method described in [13], the scattered Green's dyadic is found to have the form

$$\underline{\mathbf{g}}^{r,t} = \begin{pmatrix} g_{xx}^{r,t} & 0 & g_{xz}^{r,t} \\ 0 & g_{yy}^{r,t} & g_{yz}^{r,t} \\ g_{zx}^{r,t} & g_{zy}^{r,t} & g_{zz}^{r,t} \end{pmatrix} \tag{26}$$

where the Sommerfeld integrals are

$$g_{\alpha\beta}^r(\mathbf{r},\mathbf{r}') = \frac{1}{(2\pi)^2}\int_{-\infty}^{\infty}\int_{-\infty}^{\infty}g_{\alpha\beta}^r(q_x,q_y)\frac{e^{-p_1(z+z')}}{2p_1} \times e^{-jq\cdot(\mathbf{r}-\mathbf{r}')}dq_x dq_y. \tag{27}$$

For an isotropic surface, $g_{xz}^{r,t} = g_{yz}^{r,t} = 0$. The Green's dyadic for region 2, $\underline{\mathbf{g}}^t(\mathbf{r},\mathbf{r}')$, has the same form as for region 1, although in (27) the replacement

$$g_{\alpha\beta}^r e^{-p_1(z+z')} \rightarrow g_{\alpha\beta}^t e^{p_2 z}e^{-p_1 z'} \tag{28}$$

must be made.

In the event of general media (μ_1, ε_1 for $z \geq 0$ and μ_2, ε_2 for $z < 0$) the coefficients $g_{\alpha\beta}^{r,t}(q_x,q_y)$ are quite complicated and will be omitted here due to space limitations. The results for the special case of an isotropic surface conductivity (i.e., if $B_0 = 0$ and spatial dispersion effects are ignored) are given in [11]. Since spatial dispersion effects are shown to be small in the microwave regime, here explicit expressions will be provided for the special case of the graphene surface residing in a homogeneous space characterized by $\mu_1 = \mu_2 = \mu_b$ and $\varepsilon_1 = \varepsilon_2 = \varepsilon_b$ in the Hall regime with no spatial dispersion (i.e., using (4) as the conductivity). In this case, the coefficients in region 1 are given as

$$\begin{aligned}
g_{xx}^r(q_x,q_y) &= \frac{k^2q_ys_d - p^2q_xs_o - ipkq_y\left(s_d^2+s_o^2\right)}{q_yD(q_\rho)} &(29)\\
g_{xz}^r(q_x,q_y) &= \frac{-ips_oq_\rho^2}{2q_yD(q_\rho)} &(30)\\
g_{yy}^r(q_x,q_y) &= \frac{p^2q_ys_o + k^2q_xs_d - ipkq_x\left(s_d^2+s_o^2\right)}{q_xD(q_\rho)} &(31)\\
&= g_{xx}^r(-q_y,q_x) &(32)\\
g_{yz}^r(q_x,q_y) &= \frac{ips_oq_\rho^2}{2q_xD(q_\rho)} = -g_{xz}^r(-q_y,q_x) &(33)\\
g_{zx}^r(q_x,q_y) &= \frac{-ip\left(q_xq_ys_d + \left(k^2-q_x^2\right)s_o\right)}{q_yD(q_\rho)} &(34)\\
g_{zy}^r(q_x,q_y) &= \frac{-ip\left(q_xq_ys_d + \left(q_y^2-k^2\right)s_o\right)}{q_xD(q_\rho)} \\
&= -g_{zx}^r(-q_y,q_x) &(35)\\
g_{zz}^r(q_x,q_y) &= \frac{pq_xq_y\left(2ps_d + 2ik\left(s_d^2+s_o^2\right)\right) + p^2s_o\left(q_y^2-q_x^2\right)}{2q_xq_yD(q_\rho)} &(36)
\end{aligned}$$

where

$$\begin{aligned}
s_d &= \frac{\eta\sigma_d}{2}, \quad s_o = \frac{\eta\sigma_o}{2} \\
\eta &= \sqrt{\frac{\mu_b}{\varepsilon_b}}, \quad k = \omega\sqrt{\mu_b\varepsilon_b} &(37)\\
D(q_\rho) &= (p^2-k^2)s_d + ipk\left(1+s_d^2+s_o^2\right) \\
p &= \sqrt{q_\rho^2-k^2}. &(38)
\end{aligned}$$

In the more general case of an arbitrary graphene conductivity tensor, the results are only moderately more complicated, assuming that the graphene resides in a homogeneous space.

The factor of 2 in the denominators of the equations for $g^r_{\alpha z}$, $\alpha = x, y, z$ [i.e., (30), (33), and (36)] is a result of the z component of current producing all three components of potential π_x, π_y, and π_z. Because there is no $x-y$ coupling of potential ($g_{xy} = g_{yx} = 0$), one can derive the components $g_{\alpha z}$ by using each pair (π_x, π_z) and (π_y, π_z), adding the results, and dividing by 2 (since the source has essentially been applied twice). Alternatively, the components $g_{\alpha z}$ can be obtained using the pair (π^e_z, π^m_z), where $\pi^{e/m}_z$ is the electric/magnetic Hertzian potential [15]. To verify the final electric and magnetic fields obtained from the Hertzian potentials, the electric dyadic Green's function was derived independent of potentials, using the field method outlined in [16, Ch. 6], extended to account for cross-polarization terms (see Appendix III). Numerical tests verified that the final fields were the same in both cases for the general graphene surface. Although the field method is a bit more straightforward than the method of potentials presented here, there are several reasons why the Hertzian potential method is desirable. First, the resulting potential Green's components (e.g., $g^r_{\alpha\beta}$ presented above) are simpler than the electric field Green's components, and allow for a clear interpretation of the underlying wave physics. Second, in quantum mechanics the potential plays a dominant role in governing electron dynamics, and so a potential formulation may facilitate further work in this area.

In the lower region, the coefficients $g^t_{\alpha\beta}$ are

$$g^t_{xx}(q_x, q_y) = \frac{p^2(q_y s_d - q_x s_o) + ipkq_y}{q_y D(q_\rho)} \tag{39}$$

$$g^t_{xz}(q_x, q_y) = g^r_{xz}(q_x, q_y) \tag{40}$$

$$g^t_{yy}(q_x, q_y) = \frac{p^2(q_x s_d + q_y s_o) + ipkq_x}{q_x D(q_\rho)} \tag{41}$$

$$= g^t_{xx}(-q_y, q_x) \tag{42}$$

$$g^t_{yz}(q_x, q_y) = g^r_{yz}(q_x, q_y) \tag{43}$$

$$g^t_{zx}(q_x, q_y) = -g^r_{zx}(q_x, q_y) \tag{44}$$

$$g^t_{zy}(q_x, q_y) = -g^r_{zy}(q_x, q_y) \tag{45}$$

$$g^t_{zz}(q_x, q_y) = \frac{2kq_xq_y(ip - ks_d) + p^2 s_o\left(q_x^2 - q_y^2\right)}{2q_yq_xD(q_\rho)}. \tag{46}$$

In the general medium case, both waveparameters $p_n = \sqrt{q_\rho^2 - k_n^2}$, $n = 1, 2$, lead to branch points at $q_\rho = \pm k_n$, and thus the q_ρ-plane is a four-sheeted Riemann surface. The standard hyperbolic branch cuts [15] that separate the one proper sheet (where $\mathrm{Re}(p_n) > 0$, such that the radiation condition as $|z| \to \infty$ is satisfied) and the three improper sheets (where $\mathrm{Re}(p_n) < 0$) are the same as in the absence of surface conductivity. As in the usual layered medium theory, branch points (and the associated branch-cut integrals in a spectral representation) are associated with radiation into the surrounding medium.

C. Surface Waves Guided by Graphene

Pole singularities in the Sommerfeld integrals represent discrete surface waves guided by the medium [14], [15]. For the case of graphene having an arbitrary conductivity tensor and residing in a homogeneous medium characterized by μ_b, ε_b, surface wave poles satisfy $D(q_x, q_y) = 0$, where

$$D(q_x, q_y) = q_xq_z(\sigma_{yx} + \sigma_{xy}) + \left(q_z^2 - k^2\right)\sigma_{yy} + \left(q_x^2 - k^2\right)\sigma_{xx} + 2ip\varepsilon_b\omega\left(1 + \frac{1}{4}\eta^2(\sigma_{xx}\sigma_{yy} - \sigma_{xy}\sigma_{yx})\right). \tag{47}$$

In the Hall effect regime (i.e., using (4) as the conductivity), $D(q_x, q_y)$ simplifies to be $D(q_\rho)$ in (38), which can be solved to yield

$$q^\pm_\rho = k\left[\frac{1}{2^2 s_d^2}\left(-is^2 \pm \sqrt{4s_d^2 - s^4}\right)^2 + 1\right]^{1/2} \tag{48}$$

where $s^2 = s_d^2 + s_o^2 + 1$. For both the special case of an isotropic sheet characterized by (3), and, since σ_o is an odd function of μ_c, in the Hall regime when $\mu_c = 0$, we have $s_o = 0$, and in these cases (48) becomes

$$q^+_\rho = q^{TM}_\rho = k\sqrt{1 - \frac{1}{s_d^2}}, \quad q^-_\rho = q^{TE}_\rho = k\sqrt{1 - s_d^2}. \tag{49}$$

These correspond to the transverse-magnetic (TM, E-wave) case and the transverse-electric (TE, H-wave) case, respectively, where transverse is with respect to the radial coordinate. For isolated graphene characterized by complex surface conductivity $\sigma = \sigma' + j\sigma''$, a proper TE surface wave exists if and only if $\sigma'' > 0$ (associated with interband conductivity; see the discussion in Appendix I), and a proper TM surface wave exists for $\sigma'' < 0$ (associated with intraband conductivity). Surface-wave behavior in the isotropic case for $B_0 = 0$ was considered in [11].

III. Results

In this section, the importance of spatial dispersion will be assessed, and the effect of dc electric and magnetic bias on electromagnetic field behavior near a graphene surface in the microwave regime will be considered (due to space limitations, THz and infrared frequencies will be considered elsewhere). In all cases, results will be presented at room temperature, $T = 300$ K, and $\Gamma = 0.11$ meV ($\Gamma = 1/2\tau$; $\tau = 3$ ps); the value of the scattering rate is chosen to be approximately the same as for electron-acoustic phonon interactions in single-wall carbon nanotubes [17]. For simplicity, and to focus on the effects of the graphene surface, in the following numerical results we will assume graphene in a homogeneous medium characterized by ε_0, μ_0, and having wavenumber $k = k_0$, the free-space wavenumber. Double integrals (27) were computed in rectangular form using a Romberg integration routine. In the case of an isotropic surface impedance, it is convenient to convert to polar form since the angular integral can be performed analytically.

A. Effect of Spatial Dispersion

In the spatial dispersive regime the conductivity has the form (2), derived in Appendix II. It is easy to see that the terms asso-

ciated with α and β are quite small below THz frequencies by examining the ratio [see (96)–(101)]

$$\delta = \frac{4}{3}\frac{\alpha q_\alpha q_\beta}{\sigma} = \frac{v_F^2 q_\alpha q_\beta}{(\omega - i\tau^{-1})^2} \tag{50}$$

in the Fourier transform domain, where the term $q_\alpha q_\beta$, $\alpha, \beta = x, y$, arises from the spatial derivatives in (2), and electron velocity v_F is described in Appendix I.

The value of the wavenumbers q_α and q_β govern the size of δ, and to access upper limits for the wavenumbers it is worthwhile to represent the spectral integrals (27) as a sum of branch cuts and residues [14], [15], [18]. For propagating space-wave radiation arising from the branch cuts, all of the spectral content occurs for $|q| \leq k$. If we also assume that surface-wave propagation constants from (47) are such that $|q_\rho| \leq k$, then below the THz regime where $\omega \ll \tau^{-1}$, $|\delta| \leq (v_F k\tau)^2 = 10^{-12}k^2$, such that $|\delta| \leq 10^{-8}$ at 10 GHz (and δ obviously decreases as frequency is lowered). Thus, in this case the derivative terms associated with spatial dispersion in (2) can be ignored, and the conductivity can be modeled as isotropic in the absence of a magnetic bias field.

The assumption $|q_\rho| \leq k$ is reasonable at GHz frequencies and below, where the intraband conductivity having $\sigma_d'' < 0$ strongly dominates over the interband conductivity having $\sigma_d'' > 0$ (see Appendix I). Thus, at these frequencies only TM surface waves may propagate, the conductivity is relatively large, and from, e.g., (49), $q_\rho^{TM} \simeq k$. Thus, spatial dispersion effects seem to be unimportant below THz frequencies. The presence of a magnetic bias may change this conclusion, although even in the case of a magnetic-bias induced TE surface wave (see Fig. 8), $|q_\rho^{TE}| \leq k$, and so it is reasonable that the same conclusions hold.

In order to gauge the effect of spatial dispersion at THz frequencies and above, a procedure different than that presented in Appendix II is required, since in that treatment only the intraband conductivity is considered. This conductivity becomes comparable to, or smaller than the interband term above a few THz.

Assuming for the moment that the spatial dispersion analysis holds above THz frequencies, it is easily seen that extremely slow surfaces waves may necessitate the inclusion of spatial dispersion. For the isotropic graphene surface, it is shown in [11] that in the near-infrared, in some cases only a TE surface wave with $|q_\rho^{TE}| \simeq k$ will propagate, whereas in other situations only a TM surface wave with $|q_\rho^{TM}| \gg k$ will exist. With $|q_\rho| = ak$, since $\omega \gg \tau^{-1}$, $\delta = (av_F/c)^2$, where c is the speed of light in the medium. Assuming $c = c_0$, the speed of light in a vacuum, then $\delta \sim 10^{-5}a^2$, such that if $a \simeq 1$ (TE case), $\delta \sim 10^{-5}$, and if $a \simeq 100$ (a typical value in the TM case), $\delta \sim 0.1$. Obviously, when the condition $\delta \ll 1$ is violated, spatial dispersion effects will be important, and, since $\beta = \alpha/3$, the same comments apply to β. Thus, the existence of very slow surface waves may necessitate the inclusion of spatial dispersion.

In summary, below the THz frequency range spatial dispersion effects seem to be unimportant. Spatial dispersion may be important for surface waves with $|q_\rho| \gg |k|$, but this situation seems to occur only for moderately high THz frequencies and above, for which the development presented in Appendix II is not strictly valid.

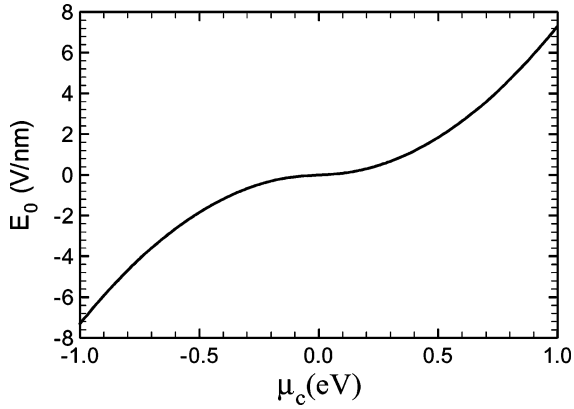

Fig. 2. The relationship between electric bias field E_0 and chemical potential μ_c obtained from (53), with $\varepsilon_b = \varepsilon_0$.

B. Effect of Electric Bias

In the electric bias regime the conductivity has the form (3). The influence of the electric bias E_0 is incorporated into the conductivity expressions via the chemical potential (through the Fermi-Dirac distribution; see Appendix I), and so a relation between chemical potential and electrostatic bias must be established. The normal displacement vector D_n on either side of a charged sheet in a homogeneous dielectric characterized by ε_b is $D_n = \varepsilon_b E_0 = en_s/2$, where n_s is the two-dimensional surface-charge density and $-e$ is the electronic charge. For an isolated graphene sheet the chemical potential μ_c is determined by the extra carrier density as [19], [20]

$$n_s = \frac{2}{\pi\hbar^2 v_F^2}\int_0^\infty \varepsilon\left(f_d(\varepsilon) - f_d(\varepsilon + 2\mu_c)\right)d\varepsilon \tag{51}$$

where

$$f_d(\varepsilon) = \left(e^{(\varepsilon-\mu_c)/k_B T} + 1\right)^{-1} \tag{52}$$

is the Fermi-Dirac distribution, ε is energy, and k_B is Boltzmann's constant (for the undoped, ungated case, $n_s = \mu_c = 0$). Thus, for a given E_0

$$\frac{2\varepsilon_b E_0}{e} = \frac{2}{\pi\hbar^2 v_F^2}\int_0^\infty \varepsilon\left(f_d(\varepsilon) - f_d(\varepsilon + 2\mu_c)\right)d\varepsilon \tag{53}$$

can be solved for the chemical potential $\mu_c(E_0)$ using a numerical root search, or, more simply, E_0 can be directly obtained for a given chemical potential (the carrier density can also be controlled by chemical doping). The relationship between bias field E_0 and chemical potential in graphene obtained from (53) is shown in Fig. 2.

It can be seen that the chemical potential can be easily tuned from -1 eV to 1 eV by typical values of bias fields that have been used in experiments [3], [4]. In these measurements, the graphene surface was supported by a dielectric substrate on a ground plane, with a voltage V_g applied across the structure. In this case, the factor $\varepsilon_b E_0$ is replaced by $\varepsilon_s V_g/d$, where ε_s is the

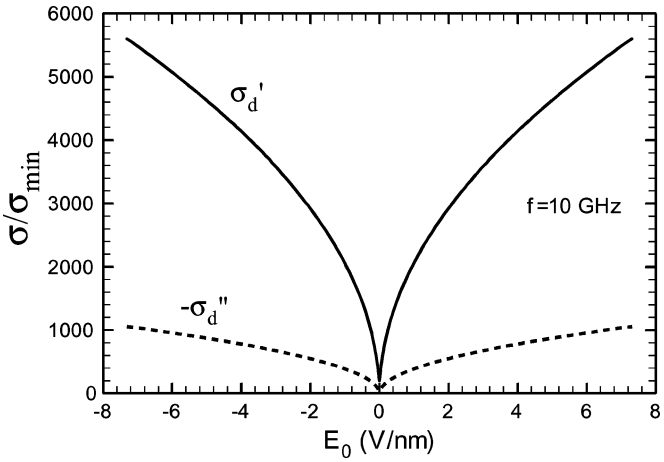

Fig. 3. Conductivity (57) as a function of applied bias field E_0 at 10 GHz. For $E_0 = \mu_c = 0$, $\sigma/\sigma_{\min} = 200.84 - j37.85$.

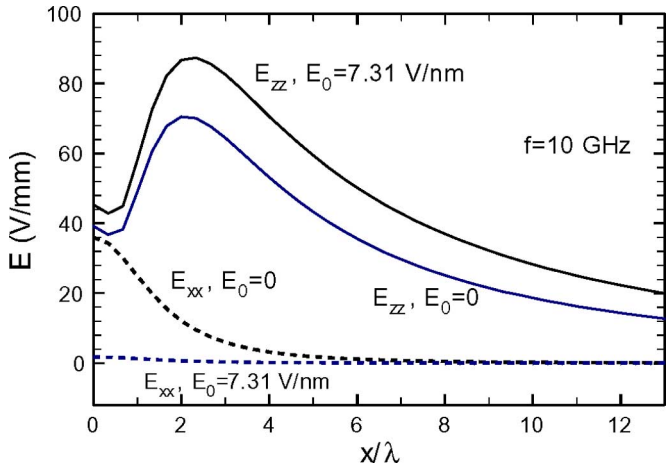

Fig. 4. Vertical electric field due to a vertical current (E_{zz}) and horizontal electric field due to a horizontal current (E_{xx}) from (5), as functions of position along the graphene surface for two different bias fields E_0. The source is located at $(x', y', z') = (0, 0, 1.67)\lambda$, and the observation point is $(x, 0, 0)$.

substrate permittivity (typically $\varepsilon_s \sim 3.9\varepsilon_0$) and d is the substrate thickness (typically $d \sim 300\,\mathrm{nm}$). Thus, for the typical experimental parameters of V_g in the range 0–100 V, $\varepsilon_s V_g/d\varepsilon_0$ is in the range 0–1 V/nF, and so bias fields E_0 on the order of several volts per nanometer are easily obtainable, and larger fields can by achieved by using thinner substrates or higher voltages. In this work, we do not have a grounded structure, and so a bias field E_0 is assumed rather than a gate voltage, but in practice this would be a gated structure where the bias voltage source provides the excess charge carriers.

The isotropic conductivity (57) (i.e., (54) with $B_0 \to 0$) as a function of electric bias field E_0 is shown in Fig. 3, where $\sigma_{\min} = \pi e^2/2h = 6.085 \times 10^{-5}$ (S). It can be seen that conductivity is significantly changed using moderate bias fields.

Fig. 4 shows the time-harmonic vertical electric field due to a vertical current (E_{zz}) and the horizontal electric field due to a horizontal current (E_{xx}) from (5), as functions of position along the graphene surface for two different bias fields E_0. The source is located at $(x', y', z') = (0, 0, 1.67)\lambda$, and the observation point is $(x, 0, 0)$. From (53), for $E_0 = 0$, $\mu_c = 0$, and for $E_0 = 7.31\ \mathrm{V/nm}$, $\mu_c = 1\ \mathrm{eV}$. It can be seen that the bias has a strong effect on the fields. The field behavior can be understood by considering that as the bias increases, more charge exists on the surface by (53), and the surface conductivity increases. Thus, as the surface becomes a better conductor, the horizontal field is shorted out, and the vertical field increases (obviously, in the limit $\sigma \to \infty$, $E_{xx} \to 0$).

C. Effect of Magnetic Bias

In the magnetic bias (Hall effect) regime where $B_0 \neq 0$, the conductivity has the form (4), with explicit expressions given by (54) and (55). In Fig. 5 the conductivity is shown as a function of magnetic bias B_0 for two different values of electric bias, $E_0 = 0.0886\ \mathrm{V/nm}$ ($\mu_c = 0.1\ \mathrm{eV}$) and $E_0 = 0$ ($\mu_c = 0$). The conductivity σ_o is an odd function of μ_c and B_0, and therefore $\sigma_o \to 0$ as $B_0 \to 0$ and $\sigma_o = 0$ for $\mu_c = 0$ regardless of the value of B_0. The small circles at $B_0 = 0$ are the values of σ_d obtained from the simple formula (58), valid in the absence of magnetic bias. It can be seen that the simple, low magnetic bias conductivities (58) and (62) are only valid for very small values of magnetic bias, since (58) is independent of B_0 and (62) is linear in B_0. From the figure, it is clear that these will only hold for $B_0 \ll 0.01$ T.

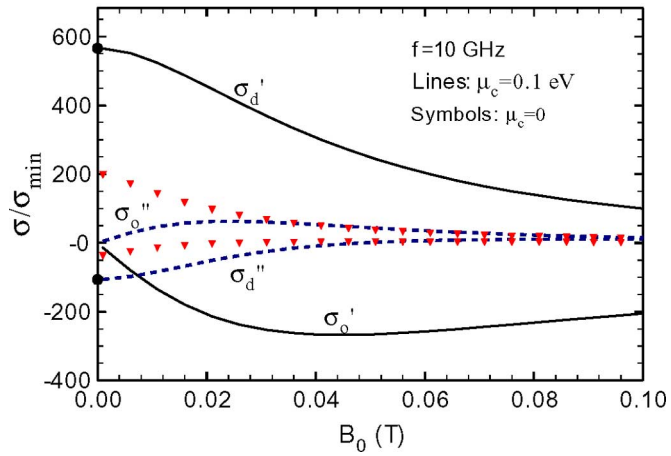

Fig. 5. Conductivity (4) as a function of magnetic bias B_0 for $E_0 = 0.0886\ \mathrm{V/nm}$ ($\mu_c = 0.1\ \mathrm{eV}$, solid and dashed lines) and for $E_0 = 0$ ($\mu_c = 0$, symbols; upper curve is σ_d', lower curve is σ_d'', and $\sigma_o = 0$). The small filled circles at $B_0 = 0$ are the values of σ_d obtained from the simple formula (58), valid in the absence of magnetic bias.

The field components E_{zz} and E_{xx} corresponding to the conductivity in Fig. 5 are shown in Fig. 6 for $B_0 = 0$, 0.08 T, and 1 T, where the electric bias is $E_0 = 0.0886\ \mathrm{V/nm}$ ($\mu_c = 0.1\ \mathrm{eV}$). As B_0 increases the conductivity tends to decrease in magnitude, in which case E_{xx} increases and E_{zz} decreases.

An interesting situation occurs for $B_0 \neq 0$ and $E_0 = \mu_c = 0$. Since graphene is a zero-gap semiconductor, in the intrinsic case ($\mu_c = 0$), as in any intrinsic semiconductor, the Hall electron current is equal and opposite to the Hall hole current, and so the conductivity is a scalar, σ_d, given by (54). Fig. 7 shows the

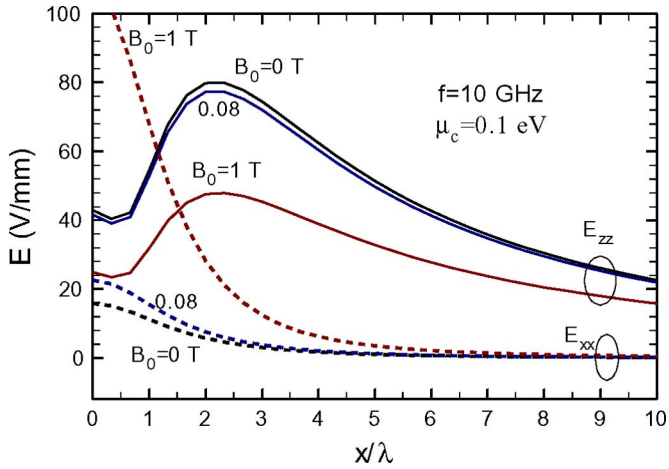

Fig. 6. Electric field components E_{zz} and E_{xx} corresponding to the conductivity in Fig. 5 for $B_0 = 0$, $B_0 = 0.08$ T, and $B_0 = 1$ T, with $E_0 = 0.0886$ V/nm ($\mu_c = 0.1$ eV).

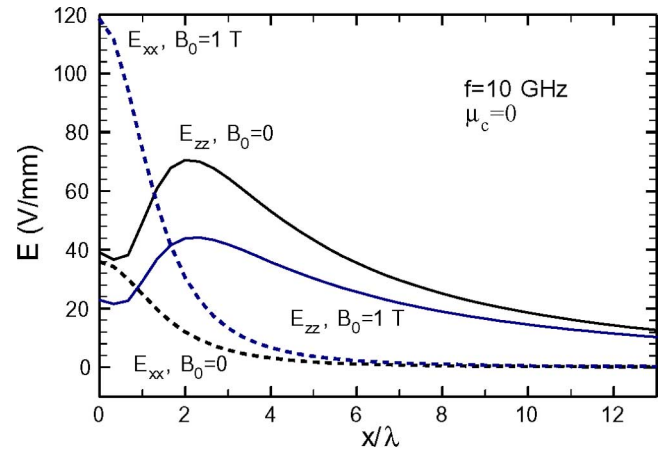

Fig. 7. Field components E_{zz} and E_{xx} for $B_0 = 0$ and $B_0 = 1$ T, when $E_0 = \mu_c = 0$ (scalar conductivity in the Hall regime).

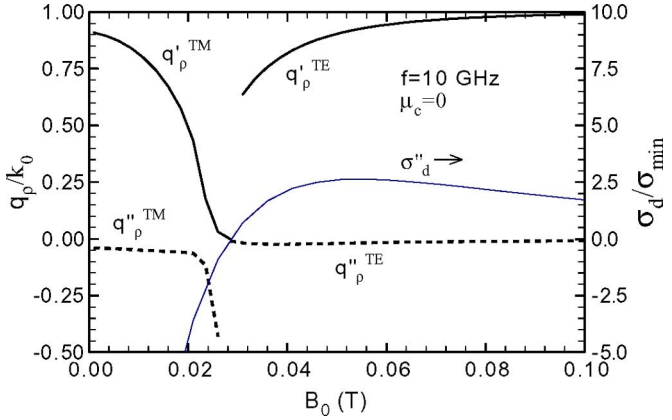

Fig. 8. Surface wave propagation constant for $E_0 = \mu_c = 0$ ($\sigma_o = 0$) at 10 GHz. For $B_0 < 0.0286$ T, $\sigma_d'' < 0$ (shown as the thin line), such that only a proper TM surface wave exists, and for $B_0 > 0.0286$ T, $\sigma_d'' > 0$, such that only a proper TE surface wave exists.

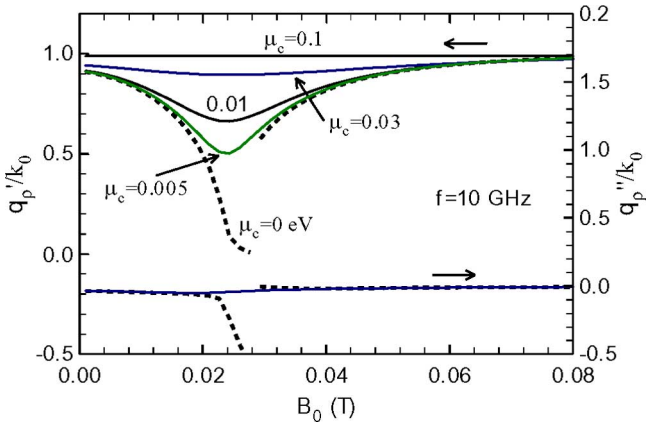

Fig. 9. Surface wave propagation constant at 10 GHz for various values of chemical potential.

difference in the E_{zz} and E_{xx} components for $B_0 = 0$ and $B_0 = 1$ T when $\mu_c = 0$.

Surface wave propagation for the electrostatic bias case ($B_0 = 0$) was discussed in [11] and [21]. For the case of magnetostatic bias, the surface wave propagation constant can be significantly affected by the bias, depending on the level of the chemical potential. In the case $E_0 = \mu_c = 0$ ($\sigma_o = 0$) at 10 GHz, the normalized surface wave propagation constant is shown in Fig. 8. In particular, referring to the conductivity in Fig. 5 for $\mu_c = 0$ (symbols), for $B_0 < 0.0286$ T, $\sigma_d'' < 0$, such that only a proper TM surface wave exists, and for $B_0 > 0.0286$ T, $\sigma_d'' > 0$, such that only a proper TE surface wave exists (the imaginary part of conductivity σ_d'' is also shown in Fig. 8 as a guide). There is a gap in the spectrum at the point where $\sigma_d'' = 0$. This can be understood from the dispersion behavior of (49). For $B_0 < 0.0286$ T, $\mathrm{Im}(q_\rho^{TE}) > 0$ and $\mathrm{Im}(q_\rho^{TM}) < 0$, so that the TM surface wave is on the proper sheet, whereas the TE surface wave is on the improper sheet. For $B_0 > 0.0286$ T, $\mathrm{Im}(q_\rho^{TE}) < 0$ and $\mathrm{Im}(q_\rho^{TM}) > 0$, so that the TM surface wave is on the improper sheet, whereas the TE surface wave is on the proper sheet. However, $\mathrm{Re}(q_\rho^{TE})/k \neq 0$ at $B_0 = 0.0286$ T, and so there is a gap in the wavenumber at this critical value of bias field.

A small electrostatic bias can change this behavior. In Fig. 9, the $\mu_c = 0$ result is shown, along with several values of chemical potential corresponding to small electrostatic bias values ($E_0 = 0.00528$ V/nm for $\mu_c = 0.01$ eV, $E_0 = 0.0886$ V/nm for $\mu_c = 0.1$ eV, etc.). For the cases $\mu_c > 0$, conductivity is not a scalar ($\sigma_o \neq 0$), and the gap in the spectrum tends to disappear as the chemical potential is increased.

IV. Conclusion

Dyadic Green's functions have been presented in terms of Sommerfeld integrals for a non-local, anisotropic, two-sided surface conductivity model of biased graphene. Either electric or magnetic bias can be applied, and used to tune the conductivity of the graphene surface. The formulation is presented for an arbitrary conductivity tensor, and explicit expressions are provided for the special case of graphene in a homogeneous medium in the Hall effect regime. It is shown that the effect of both magnetostatic and electrostatic bias on field and surface wave behavior in the microwave regime is substantial. This may

be useful for advanced applications where electronic control of electromagnetic properties is desirable.

APPENDIX I
CONDUCTIVITY COMPONENTS

The conductivities σ_d and σ_o in (3) and (4) can be determined from the Kubo formalism [22], and explicit expressions from [23, Eqs. (11) and (12)] (see also [24]–[29]) are

$$\begin{aligned}\sigma_d&(\mu_c(E_0),B_0)\\ &=\frac{e^2v_F^2|eB_0|(\omega-j2\Gamma)\hbar}{-j\pi}\\ &\quad\times\sum_{n=0}^{\infty}\left\{\frac{f_d(M_n)-f_d(M_{n+1})+f_d(-M_{n+1})-f_d(-M_n)}{(M_{n+1}-M_n)^2-(\omega-j2\Gamma)^2\hbar^2}\right.\\ &\qquad\times\left(1-\frac{\Delta^2}{M_nM_{n+1}}\right)\frac{1}{M_{n+1}-M_n}\\ &\qquad+\frac{f_d(-M_n)-f_d(M_{n+1})+f_d(-M_{n+1})-f_d(M_n)}{(M_{n+1}+M_n)^2-(\omega-j2\Gamma)^2\hbar^2}\\ &\qquad\left.\times\left(1+\frac{\Delta^2}{M_nM_{n+1}}\right)\frac{1}{M_{n+1}+M_n}\right\}\end{aligned}\tag{54}$$

and

$$\begin{aligned}\sigma_o&(\mu_c(E_0),B_0)\\ &=-\frac{e^2v_F^2eB_0}{\pi}\sum_{n=0}^{\infty}\{f_d(M_n)-f_d(M_{n+1})\\ &\qquad\qquad-f_d(-M_{n+1})+f_d(-M_n)\}\\ &\quad\times\left\{\left(1-\frac{\Delta^2}{M_nM_{n+1}}\right)\frac{1}{(M_{n+1}-M_n)^2-(\omega-j2\Gamma)^2\hbar^2}\right.\\ &\qquad\left.+\left(1+\frac{\Delta^2}{M_nM_{n+1}}\right)\frac{1}{(M_{n+1}+M_n)^2-(\omega-j2\Gamma)^2\hbar^2}\right\}\end{aligned}\tag{55}$$

where

$$M_n=\sqrt{\Delta^2+2nv_F^2|eB_0|\hbar}\tag{56}$$

and where $-e$ is the charge of an electron, $\hbar=h/2\pi$ is the reduced Planck's constant, f_d is the Fermi-Dirac distribution (52), $v_F\simeq 10^6$ m/s is the electron's energy-independent velocity (due to graphene's linear bands) [4], and Δ is an excitonic energy gap. This gap is opened due to electron interactions in the presence of a magnetic field [30], [31], and can play a significant role at low temperatures [25]. However, at higher temperature the increased carrier density enhances screening effects, which diminishes the gap [31]. Moreover, for the room temperature results considered here, energy gaps less than several hundred Kelvin (the expected range of values) are small compared to thermal energy, and their numerical inclusion resulted in no observable change in the conductivity. Therefore, all numerical results for which $B_0\neq 0$ were computed using (54) and (55) with $\Delta=0$. Furthermore, it should be noted that the conductivity expressions were derived for an isolated graphene sheet, and electronic interactions with surrounding dielectrics are ignored. Electromagnetic interactions with surrounding dielectrics are included in the derived Green's functions.

As a special case, in the low magnetic field limit for $\Delta=0$ [23, Eq. (13)]

$$\begin{aligned}\sigma_d&\left(\mu_c(E_0)\right)=\frac{je^2(\omega-j2\Gamma)}{\pi\hbar^2}\\ &\left[\frac{1}{(\omega-j2\Gamma)^2}\int_0^{\infty}\varepsilon\left(\frac{\partial f_d(\varepsilon)}{\partial\varepsilon}-\frac{\partial f_d(-\varepsilon)}{\partial\varepsilon}\right)d\varepsilon\right.\\ &\left.-\int_0^{\infty}\frac{f_d(-\varepsilon)-f_d(\varepsilon)}{(\omega-j2\Gamma)^2-4(\varepsilon/\hbar)^2}d\varepsilon\right]\end{aligned}\tag{57}$$

where the first term in (57) is due to intraband contributions, and the second term to interband contributions. (57) is particularity useful when $B_0\to 0$, since in this case (54) converges very slowly.

The intraband term in (57) can be evaluated as

$$\sigma_{d,\text{intra}}=-j\frac{e^2k_BT}{\pi\hbar^2(\omega-j2\Gamma)}\left(\frac{\mu_c}{k_BT}+2\ln\left(e^{-\frac{\mu_c}{k_BT}}+1\right)\right).\tag{58}$$

With $\sigma=\sigma'+j\sigma''$, it can be seen that $\sigma'_{d,\text{intra}}\geq 0$ and $\sigma''_{d,\text{intra}}<0$. The sign of the imaginary part of conductivity plays an important role in the propagation of surface waves guided by the graphene sheet [21].

The interband conductivity is on the order of $e^2/\hbar$ [28], and at room temperatures and for frequencies below the THz regime, the interband conductivity is very small compared to the intraband term, and usually can be ignored. In general, the interband term must be evaluated numerically, but it can be approximated for $k_BT\ll|\mu_c|,\hbar\omega$ as [32]

$$\sigma_{d,\text{inter}}\left(\mu_c(E_0)\right)\simeq\frac{-je^2}{4\pi\hbar}\ln\left(\frac{2|\mu_c|-(\omega-j2\Gamma)\hbar}{2|\mu_c|+(\omega-j2\Gamma)\hbar}\right)\tag{59}$$

such that for $\Gamma=0$ and $2|\mu_c|>\hbar\omega$, $\sigma_{inter}=j\sigma''_{d,\text{inter}}$ with $\sigma''_{d,\text{inter}}>0$. For $\Gamma=0$ and $2|\mu_c|<\hbar\omega$, $\sigma_{d,\text{inter}}$ is complex-valued, with

$$\sigma'_{d,\text{inter}}=\frac{\pi e^2}{2h}=\sigma_{\min}=6.085\times fs10^{-5}\ (\text{S})\tag{60}$$

and $\sigma''_{d,\text{inter}}>0$ for $\mu_c\neq 0$.

The Hall conductivity is [23, Eq. (14)]

$$\begin{aligned}\sigma_o&\left(\mu_c(E_0),B_0\right)=-\frac{e^2v_F^2eB_0}{\pi\hbar^2}\\ &\times\left[\frac{1}{(\omega-j2\Gamma)^2}\int_0^{\infty}\left(\frac{\partial f_d(\varepsilon)}{\partial\varepsilon}+\frac{\partial f_d(-\varepsilon)}{\partial\varepsilon}\right)d\varepsilon\right.\\ &\left.+\int_0^{\infty}\frac{1}{(\omega-j2\Gamma)^2-4(\varepsilon/\hbar)^2}d\varepsilon\right].\end{aligned}\tag{61}$$

As in (57), the first term is due to intraband contributions, and the second term to interband contributions, with the interband

term very small compared to the intraband term at room temperature and for frequencies below the THz regime. The intraband contribution can be evaluated as

$$\sigma_{o,\text{intra}} = \frac{-e^2 v_F^2 eB_0}{\pi\hbar^2(\omega - j2\Gamma)^2}\left(1 - 2\left(e^{-\frac{\mu}{k_B T}} + 1\right)^{-1}\right). \quad (62)$$

Appendix II
Conductivity Tensor in the Presence of Spatial Dispersion

In this appendix the spatially-dispersive conductivity tensor (2) is derived. Although the procedure follows a well-known general method [22, pp. 106-111] that has been applied to carbon nanotubes in [12], the expression (2) is believed new and so it's derivation is outlined here. The starting point is Boltzmann's equation

$$\frac{\partial f}{\partial t} + \mathbf{v}\cdot\nabla_{\mathbf{r}} f - \frac{e}{\hbar}(\mathbf{E} + \mathbf{v}\times\mathbf{B})\cdot\nabla_{\mathbf{k}} f = -\frac{f - f_0}{\tau} \quad (63)$$

where $f = f(\mathbf{r}, \mathbf{k}, t)$ is the electron distribution function (i.e., the probability of finding an electron at position $\mathbf{r}$ at time t, and having quasi-momentum $\hbar\mathbf{k}$), and where $f_0 = f_d(\varepsilon(\mathbf{k}))$ is the equilibrium Fermi distribution (52) evaluated at energy ε (for undoped, unbiased graphene, $\mu_c = 0$), which is position and time-independent

$$\mathbf{v} = \mathbf{v}(\mathbf{k}) = \frac{d\mathbf{r}}{dt} = \frac{1}{\hbar}\nabla_{\mathbf{k}}\varepsilon \quad (64)$$

is the electron velocity, and

$$\mathbf{F}(\mathbf{r}, t) = -\frac{e}{\hbar}\left(\mathbf{E}(\mathbf{r}, t) + \mathbf{v}\times\mathbf{B}(\mathbf{r}, t)\right) = \hbar\frac{d\mathbf{k}}{dt} = \frac{d\mathbf{p}}{dt} \quad (65)$$

is the force on the electron.

Following the standard perturbation procedure, assume $f = f_0 + f_1$ where $|f_1| \ll f_0$ is the change in the distribution function due to the small, time-varying force $\mathbf{F}$. We assume that the time and spatial variation of the perturbation f_1 follows that of the applied field.

Using the Fourier transform (15), noting the time-dependence $e^{j\omega t}$ and that

$$\nabla_{\mathbf{k}} f_0(\mathbf{k}) = \frac{\partial f_0}{\partial E}\nabla_{\mathbf{k}}\varepsilon = \frac{\partial f_0}{\partial E}\hbar\mathbf{v} \quad (66)$$

$$\nabla_{\mathbf{r}} e^{-j\mathbf{q}\cdot\mathbf{r}} = -j\mathbf{q}e^{-j\mathbf{q}\cdot\mathbf{r}} \quad (67)$$

and keeping only first-order terms, it is easy to show that

$$f_1(\mathbf{k}, \mathbf{q}, \omega) = \frac{-je\mathbf{E}(\mathbf{q}, \omega)\cdot\mathbf{v}(\mathbf{k})\frac{\partial f_0}{\partial\varepsilon}}{\omega - \mathbf{v}(\mathbf{k})\cdot\mathbf{q} - j\tau^{-1}}. \quad (68)$$

The requirement for $\mathbf{E}$ to be small results from the requirement for f_1 to be small. Ignoring spatial dispersion comes from ignoring the term

$$\mathbf{v}\cdot\nabla_{\mathbf{r}} f = \mathbf{v}\cdot\nabla_{\mathbf{r}}(f_0 + f_1 e^{-j\mathbf{q}\cdot\mathbf{r}}) \quad (69)$$

which implies that the perturbation from equilibrium of the electron's distribution function due to the applied field is independent of position.

The current density in the Fourier transform domain is

$$\begin{aligned}\mathbf{J}(\mathbf{q}, \omega) &= \frac{-2e}{(2\pi)^2}\iint \mathbf{v}(\mathbf{k}) f_1 d^2\mathbf{k} \\ &= \frac{j2e^2}{(2\pi)^2}\iint \mathbf{v}(\mathbf{k})\left(\frac{\mathbf{E}(\mathbf{q}, \omega)\cdot\mathbf{v}(\mathbf{k})\frac{\partial f_0}{\partial\varepsilon}}{\omega - \mathbf{v}\cdot\mathbf{q} - j\tau^{-1}}\right) d^2\mathbf{k} \quad (70)\end{aligned}$$

since no current flows from the equilibrium distribution. The hole current is obtained in the same manner, and so the total conductivity dyadic is

$$\boldsymbol{\sigma}(\mathbf{q}, \omega) = \frac{j4e^2}{(2\pi)^2}\int\int \frac{\mathbf{vv}}{\omega - \mathbf{v}\cdot\mathbf{q} - j\tau^{-1}}\frac{\partial f_0(\mathbf{k})}{\partial\varepsilon} d^2\mathbf{k} \quad (71)$$

and, thus

$$\sigma_{\alpha\beta} = \frac{j4e^2}{(2\pi)^2}\int\int \frac{v_\alpha(\mathbf{k}) v_\beta(\mathbf{k})}{\omega - \mathbf{v}\cdot\mathbf{q} - j\tau^{-1}}\frac{\partial f_0(\mathbf{k})}{\partial\varepsilon} d^2\mathbf{k} \quad (72)$$

with $\sigma_{yx} = \sigma_{xy}$. For the special case $\mathbf{q} = \mathbf{0}$ (i.e., neglecting spatial dispersion), $\sigma_{yx} = \sigma_{xy} = 0$ since v_x and v_y are odd in k_x and k_y, respectively [see (88)], and the limits of integration are symmetric. In the presence of spatial dispersion, the material response is anisotropic, as is well known [33].

To evaluate (72), we assume the long wavelength case and perform a power series expansion in terms of the small parameter $\mathbf{v}\cdot\mathbf{q}$

$$\begin{aligned}\frac{1}{\omega - (v_x q_x + v_y q_y) - i\tau^{-1}} &= \frac{1}{\omega - i\tau^{-1}} + \frac{q_x v_x + q_y v_y}{(\omega - i\tau^{-1})^2} \\ &+ \frac{2q_x q_y v_x v_y + q_x^2 v_x^2 + q_y^2 v_y^2}{(\omega - i\tau^{-1})^3} + O(q^3). \quad (73)\end{aligned}$$

The expansion will certainly be valid if $|\mathbf{v}||\mathbf{q}| \ll |\omega - j\tau^{-1}|$, such that $|\mathbf{v}| \ll v_p|1 - j(\tau\omega)^{-1}|$. Since the main contribution to the electron velocity is the Fermi velocity $|\mathbf{v}| \simeq v_F \sim 10^6$ m/s, if the phase velocity of the electromagnetic wave is $v_p \sim c$, then this relation is always satisfied. If, e.g., $v_p \sim v_F$, then we need $\omega \ll \tau^{-1} \simeq 10^{12}$ s^{-1}

Upon keeping the first non-zero terms and making the replacements $q_x^2 \to d^2/dx^2$, $q_y^2 \to d^2/dy^2$

$$\sigma_{xx} = \sigma_{xx}^0 + \alpha_{xx}\frac{\partial^2}{\partial x^2} + \alpha_{xy}\frac{\partial^2}{\partial y^2} \quad (74)$$

$$\sigma_{xy} = 2\alpha_{xy}\frac{\partial^2}{\partial x\partial y} \quad (75)$$

$$\sigma_{yx} = \sigma_{xy} \quad (76)$$

$$\sigma_{yy} = \sigma_{yy}^0 + \alpha_{xy}\frac{\partial^2}{\partial x^2} + \alpha_{yy}\frac{\partial^2}{\partial y^2} \quad (77)$$

where

$$\sigma_{xx}^0 = \alpha_0\int\int v_x^2\frac{\partial f_0}{\partial\varepsilon} d^2\mathbf{k} = \alpha_0 I_{xx}^0 \quad (78)$$

$$\sigma_{yy}^0 = \alpha_0\int\int v_y^2\frac{\partial f_0}{\partial\varepsilon} d^2\mathbf{k} = \alpha_0 I_{yy}^0 \quad (79)$$

$$\alpha_{xx} = \alpha_1\int\int v_x^4\frac{\partial f_0}{\partial\varepsilon} d^2\mathbf{k} = \alpha_1 I_{xx} \quad (80)$$

$$\alpha_{xy} = \alpha_1\int\int v_x^2 v_y^2\frac{\partial f_0}{\partial\varepsilon} d^2\mathbf{k} = \alpha_1 I_{xy} \quad (81)$$

$$\alpha_{yy} = \alpha_1 \int\int v_y^4 \frac{\partial f_0}{\partial \varepsilon} d^2\mathbf{k} = \alpha_1 I_{yy} = \alpha_{xx} \tag{82}$$

$$\alpha_0 = \frac{j4e^2}{(2\pi)^2(\omega - i\tau^{-1})}, \quad \alpha_1 = \frac{j4e^2}{(2\pi)^2(\omega - i\tau^{-1})^3}. \tag{83}$$

To evaluate the integrals, note that

$$\frac{\partial f_0}{\partial \varepsilon} = \frac{-1}{4k_B T \cosh^2\left(\frac{\varepsilon}{2k_B T}\right)} \tag{84}$$

and

$$\mathbf{v} = \frac{1}{\hbar}\nabla_{\mathbf{k}}\varepsilon = \left(\hat{\mathbf{x}}\frac{\partial}{\partial p_x} + \hat{\mathbf{y}}\frac{\partial}{\partial p_y}\right)\varepsilon(\mathbf{p}) \tag{85}$$

where $\mathbf{p} = \hbar\mathbf{k}$ is quasi-momentum. The specific aspects of graphene are incorporated via the energy function $\varepsilon(\mathbf{p})$. For graphene in the vicinity of the Dirac points (which supply the main contribution to the integral) [10]

$$\varepsilon(\mathbf{p}) = v_F|\mathbf{p} - \mathbf{p}_F| = v_F\sqrt{(p_x - p_{xF})^2 + (p_y - p_{yF})^2} \tag{86}$$

so that

$$\mathbf{v} = v_F\left(\hat{\mathbf{x}}\frac{(p_x - p_{xF})}{|\mathbf{p} - \mathbf{p}_F|} + \hat{\mathbf{y}}\frac{(p_y - p_{yF})}{|\mathbf{p} - \mathbf{p}_F|}\right). \tag{87}$$

Upon defining a coordinate system centered at $\mathbf{p}_F$ (at which point $\varepsilon = 0$), noting that the radial coordinate is $\rho = |\mathbf{P}| = \sqrt{p_x^2 + p_y^2} = \varepsilon/v_F$, with $dp_x dp_y = \rho d\rho d\phi = \varepsilon d\varepsilon d\phi / v_F^2$ and

$$\mathbf{v} = v_F\left(\hat{\mathbf{x}}\frac{p_x}{|\mathbf{p}|} + \hat{\mathbf{y}}\frac{p_y}{|\mathbf{p}|}\right) \tag{88}$$

and

$$p_x = \rho\cos\phi, \quad p_y = \rho\sin\phi \tag{89}$$

the first integral is easily evaluated as

$$I_{xx}^0 = \frac{2}{\hbar^2}\int_0^{\infty}\cos^2\phi d\phi \int_0^{2\pi}\frac{-\varepsilon}{4k_B T\cosh^2\left(\frac{\varepsilon}{2k_B T}\right)}d\varepsilon = \pi I_0. \tag{90}$$

The factor of 2 comes from having two in-equivalent Dirac points, and

$$I_0 = -\frac{2\ln(2)k_B T}{\hbar^2}. \tag{91}$$

In a similar manner

$$I_{yy}^0 = I_0\int_0^{2\pi}\sin^2\phi d\phi = I_{xx}^0 \tag{92}$$

$$I_{xx} = I_0 v_F^2\int_0^{2\pi}\cos^4\phi d\phi = \frac{3}{4}v_F^2\pi I_0 \tag{93}$$

$$I_{yy} = I_{xx} \tag{94}$$

$$I_{xy} = I_0 v_F^2\int_0^{2\pi}\cos^2\phi\sin^2\phi d\phi = \frac{1}{4}v_F^2\pi I_0 \tag{95}$$

and therefore

$$\sigma_{xx} = \sigma + \alpha\frac{\partial^2}{\partial x^2} + \beta\frac{\partial^2}{\partial y^2} \tag{96}$$

$$\sigma_{xy} = 2\beta\frac{\partial^2}{\partial x\partial y} \tag{97}$$

$$\sigma_{yx} = \sigma_{xy} \tag{98}$$

$$\sigma_{yy} = \sigma + \beta\frac{\partial^2}{\partial x^2} + \alpha\frac{\partial^2}{\partial y^2} \tag{99}$$

where

$$\sigma = \frac{-j2\ln(2)e^2 k_B T}{\pi(\omega - i\tau^{-1})\hbar^2} \tag{100}$$

$$\alpha = \frac{3}{4}\frac{v_F^2}{(\omega - i\tau^{-1})^2}\sigma, \quad \beta = \frac{1}{3}\alpha. \tag{101}$$

It can be seen that (100) agrees with (58) for $\mu_c = 0$.

Appendix III
Alternate Method for Obtaining the Dyadic Green's Functions

The reasons for using the Hertzian potential method for deriving the dyadic Green's functions are discussed in the paper. In this appendix an alternative field method is provided, since it is somewhat more straightforward, and may therefore be of interest. The method is detailed in [16] for isotropic media, and applied to the case of a one-sided anisotropic impedance surface in [34]. Here we merely briefly outline the method to the two-sided anisotropic impedance surface case.

The fields in each region are

$$\mathbf{E}^{(n)}(\mathbf{r}) = -j\omega\mu_n\int_{\Omega}\underline{\mathbf{G}}_e^{(n)}(\mathbf{r},\mathbf{r}')\cdot\mathbf{J}(\mathbf{r}')d\Omega' \tag{102}$$

$$\mathbf{H}^{(n)}(\mathbf{r}) = \int_{\Omega}\underline{\mathbf{G}}_m^{(n)}(\mathbf{r},\mathbf{r}')\cdot\mathbf{J}(\mathbf{r}')d\Omega' \tag{103}$$

where, assuming a source in region 1

$$\underline{\mathbf{G}}_e^{(1)} = \underline{\mathbf{G}}_0^{(1)} + \underline{\mathbf{G}}_s^{(1)}, \quad \underline{\mathbf{G}}_e^{(2)} = \underline{\mathbf{G}}_t^{(2)} \tag{104}$$

$$\underline{\mathbf{G}}_0^{(1)} = \left(\underline{\mathbf{I}} + \frac{\nabla\nabla}{k_1^2}\right)g, \quad g = \frac{e^{-jkR}}{4\pi R} \tag{105}$$

$$\underline{\mathbf{G}}_m^{(n)} = \nabla\times\underline{\mathbf{G}}_e^{(n)}. \tag{106}$$

The Green's dyadics can be written as

$$\begin{aligned}\underline{\mathbf{G}}_0^{(1)} = &-\hat{\mathbf{z}}\hat{\mathbf{z}}\delta(\mathbf{r} - \mathbf{r}') - \frac{j}{2(2\pi)^2}\int\int dq_x dq_y\frac{1}{k_{1z}}\\ &\times\left\{\left[\hat{\mathbf{t}}_1^{\pm}e^{-j\mathbf{k}_1^{\pm}\cdot\mathbf{r}}\right]\left[\hat{\mathbf{t}}_1^{\pm}e^{j\mathbf{k}_1^{\pm}\cdot\mathbf{r}'}\right]\right.\\ &\left.+\left[\hat{\mathbf{p}}_1^{\pm}e^{-j\mathbf{k}_1^{\pm}\cdot\mathbf{r}}\right]\left[\hat{\mathbf{p}}_1^{\pm}e^{j\mathbf{k}_1^{\pm}\cdot\mathbf{r}}\right]\right\}\end{aligned} \tag{107}$$

$$\begin{aligned}\underline{\mathbf{G}}_s^{(1)} = &-\frac{j}{2(2\pi)^2}\int\int dq_x dq_y\frac{1}{k_{1z}}\\ &\times\left\{r_{tt}\hat{\mathbf{t}}_1^{+}\hat{\mathbf{t}}_1^{-} + r_{tp}\hat{\mathbf{t}}_1^{+}\hat{\mathbf{p}}_1^{-} + r_{pt}\hat{\mathbf{p}}_1^{+}\hat{\mathbf{t}}_1^{-}\right.\\ &\left.+r_{pp}\hat{\mathbf{p}}_1^{+}\hat{\mathbf{p}}_1^{-}e^{-j\mathbf{k}_1^{+}\cdot\mathbf{r}}e^{j\mathbf{k}_1^{-}\cdot\mathbf{r}'}\right\}\end{aligned} \tag{108}$$

$$\underline{\mathbf{G}}_t^{(2)} = -\frac{j}{2(2\pi)^2}\int\int dq_x dq_y \frac{1}{k_{1z}} \times \left\{ t_{tt}\hat{\mathbf{t}}_2^-\hat{\mathbf{t}}_1^- + t_{tp}\hat{\mathbf{t}}_2^-\hat{\mathbf{p}}_1^- + t_{pt}\hat{\mathbf{p}}_2^-\hat{\mathbf{t}}_1^- + t_{pp}\hat{\mathbf{p}}_2^-\hat{\mathbf{p}}_1^- e^{-j\mathbf{k}_2^-\cdot\mathbf{r}} e^{j\mathbf{k}_1^-\cdot\mathbf{r}'} \right\} \quad (109)$$

where in (107) the upper sign is for $z > z'$, and the lower sign for $z < z'$. In these expressions

$$\mathbf{k}_n^{\pm} = \hat{\mathbf{x}}q_x + \hat{\mathbf{y}}q_y \pm \hat{\mathbf{z}}k_{nz} \quad (110)$$

$$\hat{\mathbf{t}}_n^{\pm} = \frac{\hat{\mathbf{z}}\times\hat{\mathbf{k}}_n^{\pm}}{\left|\hat{\mathbf{z}}\times\hat{\mathbf{k}}_n^{\pm}\right|}, \quad \hat{\mathbf{p}}_n^{\pm} = \hat{\mathbf{k}}_n^{\pm}\times\hat{\mathbf{t}}_n^{\pm} \quad (111)$$

where, since $|\mathbf{k}_1^{\pm}| = k_1$, $k_{nz} = \sqrt{k_n^2 - q_x^2 - q_y^2}$ ($jk_{nz} = p_n$ in the notation in (12)). The boundary conditions are

$$\hat{\mathbf{z}}\times\left[\mu_2\underline{\mathbf{G}}_t^{(2)} - \mu_1\left(\underline{\mathbf{G}}_0^{(1)} + \underline{\mathbf{G}}_s^{(1)}\right)\right] = \underline{\mathbf{0}} \quad (112)$$

$$-\hat{\mathbf{z}}\times\left[\nabla\times\underline{\mathbf{G}}_t^{(2)} - \nabla\times\left(\underline{\mathbf{G}}_0^{(1)} + \underline{\mathbf{G}}_s^{(1)}\right)\right] = -j\omega\mu_2\underline{\boldsymbol{\sigma}}\cdot\underline{\mathbf{G}}_t^{(2)} \quad (113)$$

at $z = 0$, leading to eight equations in the eight unknowns $r_{\alpha\beta}$, $t_{\alpha\beta}$.

REFERENCES

[1] A. K. Geim and K. S. Novoselov, "The rise of graphene," *Nature Materials*, vol. 6, pp. 183–191, 2007.

[2] R. Saito, G. Dresselhaus, and M. S. Dresselhaus, *Physical Properties of Carbon Nanotubes*. London, U.K.: Imperial College Press, 2003.

[3] K. S. Novoselov, A. K. Geim, S. V. Morozov, D. Jiang, Y. Zhang, S. V. Dubonos, I. V. Grigorieva, and A. A. Firsov, "Electric field effect in atomically thin carbon films," *Science*, vol. 306, pp. 666–669, 2004.

[4] K. S. Novoselov, A. K. Geim, S. V. Morozov, D. Jiang, M. I. Katsnelson, I. V. Grigorieva, S. V. Dubonos, and A. A. Firsov, "Two-dimensional gas of massless Dirac fermions in graphene," *Nature*, vol. 438, pp. 197–200, 2005.

[5] Y. Zhang, J. P. Small, W. V. Pontius, and P. Kim, "Fabrication and electric-field-dependent transport measurements of mesoscopic graphite devices," *Appl. Phys. Lett.*, vol. 86, p. 073104 (1-3), 2005.

[6] C. Berger, Z. Song, X. Li, X. Wu, N. Brown, C. Naud, D. Mayou, T. Li, J. Hass, A. N. Marchenkov, E. H. Conrad, P. N. First, and W. A. de Heer, "Electronic confinement and coherence in patterned epitaxial graphene," *Science*, vol. 312, pp. 1191–1196, 2006.

[7] Y. Zhang, Y.-W. Tan, H. L. Stormer, and P. Kim, "Experimental observation of the quantum Hall effect and Berry's phase in graphene," *Nature*, vol. 438, pp. 201–204, 2005.

[8] C. Berger, Z. Song, T. Li, X. Li, A. Y. Ogbazghi, R. Feng, Z. Dai, A. N. Marchenkov, E. H. Conrad, P. N. First, and W. A. de Heer, "Ultrathin epitaxial graphite: 2D electron gas properties and a route toward graphene-based nanoelectronics," *J. Phys. Chem.*, vol. 108, pp. 19912–19916, 2004.

[9] Y. Ouyang, Y. Yoon, J. K. Fodor, and J. Guo, "Comparison of performance limits for carbon nanoribbon and carbon nanotube transistors," *Appl. Phys. Lett.*, vol. 89, p. 203107 (1-3), 2006.

[10] P. R. Wallace, "The band theory of graphite," *Phys. Rev.*, vol. 71, pp. 622–634, 1947.

[11] G. W. Hanson, "Dyadic green's functions and guided surface waves for a surface conductivity model of graphene," *J. Appl. Phys.*, to be published.

[12] G. Y. Slepyan, S. A. Maksimenko, A. Lakhtakia, O. Yevtushenko, and A. V. Gusakov, "Electrodynamics of carbon nanotubes: Dynamic conductivity, impedance boundary conditions, and surface wave propagation," *Phys. Rev. B*, vol. 60, pp. 17136–17149, 1999.

[13] J. S. Bagby and D. P. Nyquist, "Dyadic Green's functions for integrated electronic and optical circuits," *IEEE Trans. Microwave Theory Tech.*, vol. 35, pp. 207–210, 1987.

[14] W. C. Chew, *Waves and Fields in Inhomogeneous Media*. Piscataway, NJ: IEEE Press, 1999.

[15] A. Ishimaru, *Electromagnetic Wave Propagation, Radiation, and Scattering*. Englwood Cliffs, NJ: Prentice Hall, 1991.

[16] S. K. Chu, *Electromagnetic Scattering*. New York: Springer-Verlag, 1990.

[17] R. A. Jishi, M. S. Dresselhaus, and G. Dresselhaus, "Electron-phonon coupling and the electrical conductivity of fullerene nanotubules," *Phys. Rev. B*, vol. 48, pp. 11385–11389, 1993.

[18] G. W. Hanson, "On the applicability of the surface impedance integral equation for optical and near infrared copper dipole antennas," *IEEE Trans. Antennas Propag.*, vol. 54, pp. 3677–3685, Dec. 2006.

[19] V. Ryzhii, A. Satou, and T. Otsuji, "Plasma waves in two-dimensional electron-hole system in gated graphene heterostructures," *J. Appl. Phys.*, vol. 101, p. 024509 (1-5), 2007.

[20] L. A. Falkovsky, "Unusual field and temperature dependence of the Hall effect in graphene," *Phys. Rev. B*, vol. 75, p. 033409 (1-4), 2007.

[21] S. A. Mikhailov and K. Ziegler, "A new electromagnetic mode in graphene," *Phys. Rev. Lett.*, vol. 99, p. 016803 (1-4), 2007.

[22] M. Dressel and G. Grüner, *Electrodynamics of Solids*. Cambridge, U.K.: Cambridge Univ. Press, 2002.

[23] V. P. Gusynin, S. G. Sharapov, and J. P. Carbotte, "Magneto-optical conductivity in graphene," *J. Phy. Condens. Matter*, vol. 19, p. 026222 (1-25), 2007.

[24] V. P. Gusynin and S. G. Sharapov, "Transport of Dirac quasiparticles in graphene: Hall and optical conductivities," *Phy. Rev. B.*, vol. 73, p. 245411 (1-18), 2006.

[25] V. P. Gusynin, S. G. Sharapov, and J. P. Carbotte, "Unusual microwave response of Dirac quasiparticles in graphene," *Phys. Rev. Lett.*, vol. 96, p. 256802 (1-4), 2006.

[26] N. M. R. Peres, F. Guinea, and A. H. Castro Neto, "Electronic properties of disordered two-dimensional carbon," *Phys. Rev. B*, vol. 73, p. 125411 (1-23), 2006.

[27] N. M. R. Peres, A. H. Castro Neto, and F. Guinea, "Conductance quantization in mesoscopic graphene," *Phys. Rev. B*, vol. 73, p. 195411 (1-8), 2006.

[28] K. Ziegler, "Minimal conductivity of graphene: Nonuniversal values from the Kubo formula," *Phys. Rev. B*, vol. 75, p. 233407 (1-4), 2007.

[29] L. A. Falkovsky and A. A. Varlamov, "Space-time dispersion of graphene conductivity," *Eur. Phys. J. B*, vol. 56, pp. 281–284, 2007.

[30] D. V. Khveshchenko, "Magnetic-field-induced insulating behavior in highly oriented pyrolitic graphite," *Phys. Rev. Letts.*, vol. 87, p. 206401 (1-4), 2001.

[31] E. V. Gorbar, V. P. Gusynin, V. A. Miransky, and I. A. Shovkovy, "Magnetic field driven metal-insulator phase transition in planar systems," *Phys. Rev. B*, vol. 66, p. 045108 (1-22), 2002.

[32] V. P. Gusynin, S. G. Sharapov, and J. P. Carbotte, "Sum rules for the optical and Hall conductivity in graphene," *Phys. Rev. B*, vol. 75, p. 165407 (1-12), 2007.

[33] V. M. Agranovich, *Spatial Dispersion in Crystal Optics and the Theory of Excitons*. New York: Wiley, 1966.

[34] A. Lakhtakia, "Green's functions and Brewster condition for a halfspace bounded by an anisotropic impedance plane," *Int. J. Infrared Millimeter Waves*, vol. 13, pp. 161–170, 1992.

George W. Hanson (S'85–M'91–SM'98) was born in Glen Ridge, NJ, in 1963. He received the B.S.E.E. degree from Lehigh University, Bethlehem, PA, the M.S.E.E. degree from Southern Methodist University, Dallas, TX, and the Ph.D. degree from Michigan State University, East Lansing, in 1986, 1988, and 1991, respectively.

From 1986 to 1988, he was a Development Engineer with General Dynamics, Fort Worth, TX, where he worked on radar simulators. From 1988 to 1991, he was a Research and Teaching Assistant in the Department of Electrical Engineering, Michigan State University. He is currently an Associate Professor of electrical engineering and computer science at the University of Wisconsin in Milwaukee. His research interests include nanoelectromagnetics, mathematical methods in electromagnetics, electromagnetic wave phenomena in layered media, integrated transmission lines, waveguides, and antennas, and leaky wave phenomena.

Dr. Hanson is a member of URSI Commission B, Sigma Xi, and Eta Kappa Nu. He was an Associate Editor for the IEEE TRANSACTIONS ON ANTENNAS AND PROPAGATION from 2002 to 2007. In 2006, he received the S. A. Schelkunoff Best Paper Award from the IEEE Antennas and Propagation Society.